Candida albicans END3 Mediates Endocytosis and Has Subsequent Roles in Cell Wall Integrity, Morphological Switching, and Tissue Invasion

Christiane Rollenhagen,[a,b] Harrison Agyeman,[a] Susan Eszterhas,[a,c] Samuel A. Lee[a,b]

[a]Medicine Service, White River Junction VA Medical Center, White River Junction, Vermont, USA
[b]Geisel School of Medicine at Dartmouth, Hanover, New Hampshire, USA
[c]Dartmouth College, Hanover, New Hampshire, USA

ABSTRACT The role of endocytosis in *Candida albicans* secretion, filamentation, and virulence remains poorly understood, despite its importance as a fundamental component of intracellular trafficking. Given that secretory mutants display defects in endocytosis, we have focused our attention on endocytic mutants to understand the interconnection between endocytosis and other secretory pathways. Using a reverse-genetic approach based upon CRISPR-Cas9 mediated gene deletion, we studied the functions of the gene *END3*, which plays a key role in clathrin-based endocytosis. In the *end3Δ/Δ* null mutant, clathrin-mediated endocytosis was substantially reduced. While *in vitro* growth, cell morphology, and vacuoles appeared normal, the mutant was impaired in actin patch formation, filamentous growth, biofilm formation, cell wall integrity, and extracellular protease secretion. In addition, susceptibility to various antifungal agents was altered. Consistent with the inability to form hyphae, in an *in vitro* keratinocyte infection model, the null mutant displayed reduced damage of mammalian adhesion zippers and host cell death. Thus, *C. albicans END3* has a role in efficient endocytosis that is required for cell wall integrity, protein secretion, hyphal formation, and virulence-related processes. These findings suggest that impaired endocytosis subsequently affects other secretory pathways, providing evidence of the interconnection between these processes.

IMPORTANCE *Candida albicans* is a fungal commensal organism that can cause serious opportunistic infections in immunocompromised patients leading to substantial complications and mortality. A better understanding of the microbe's biology to develop more effective therapeutic and diagnostic tools is required as invasive candidiasis is a problem of continued clinical importance. This study focuses on endocytosis, an important but incompletely understood cellular mechanism needed to uptake nutrients and communicate with a cell's environment. In this study, we have assessed the role of endocytosis in cell wall integrity, biofilm formation, and tissue invasion in *C. albicans*. These findings will improve our understanding of cellular mechanisms underlying endocytosis and will inform us of the interconnection with other intracellular transport processes.

KEYWORDS *Candida albicans*, biofilm, filamentation, pathogenesis, secretion, trafficking, virulence

Endocytosis is an essential component of the secretory pathway in eukaryotic cells and is needed for many aspects of cellular functioning, such as uptake of nutrients, extracellular signaling, and for the regulation of plasma membrane as well as cell wall composition. This highly orchestrated process begins at the cell wall and plasma membrane with vesicle formation that transports cargo into the cell. The best-characterized and most selective endocytic process is clathrin-based endocytosis (CME) which allows receptor-mediated cargo to enter the cell in an energy dependent manner (1, 2).

CME has been extensively studied in *Saccharomyces cerevisiae* (*Sc*) and requires more than 50 proteins (reviewed in Goode et al., 2015 [1]). The early-coat proteins in this process define endocytic-site location and cargo recruitment (3) while the middle and late-coat proteins induce membrane invagination and facilitate vesicle scission, in part by inducing actin assembly (4). The early-coat proteins include clathrin, the AP-2 adaptor protein, Ede1p, Syp1p, and Pal1p. Ede1p, an Eps15 homology (EH) domain protein, is one of the earliest proteins recruited to endocytic sites and facilitates site initiation and stabilization (5). While Ede1p and Syp1p remain associated with the plasma membrane, clathrin, AP-2p, and Pal1p are internalized along with the clathrin coat (6). The recruitment of Sla2 plays a key role in the transition to form the middle coat. Its ANTH domain binds to the ENTH domain of the epsins Ent1p and Ent2p. These epsins facilitate membrane bending via interactions with the polarity-establishing GTPase Cdc42p in the presence of phosphotidylinositol 4,5-bisphosphate (PIP$_2$) (7–9). The middle-coat proteins recruit the central late-coat proteins setting the stage for actin assembly that facilitates membrane invagination and vesicle scission (10). Key late-coat proteins include Pan1p, Sla1p, Prk1p, End3p, and Las17p. Their assembly is concluded when Las17p is recruited to endocytic sites partially through its interaction with Sla1p (11). The late coat assembly provides the foundation for subsequent membrane invagination and endocytosis. Pan1p is the only endocytic protein essential for viability in this pathway and provides a major contribution to actin cytoskeletal organization by binding Arp2/3p, F-actin, and type-I myosin motors with its EH domains (12–14).
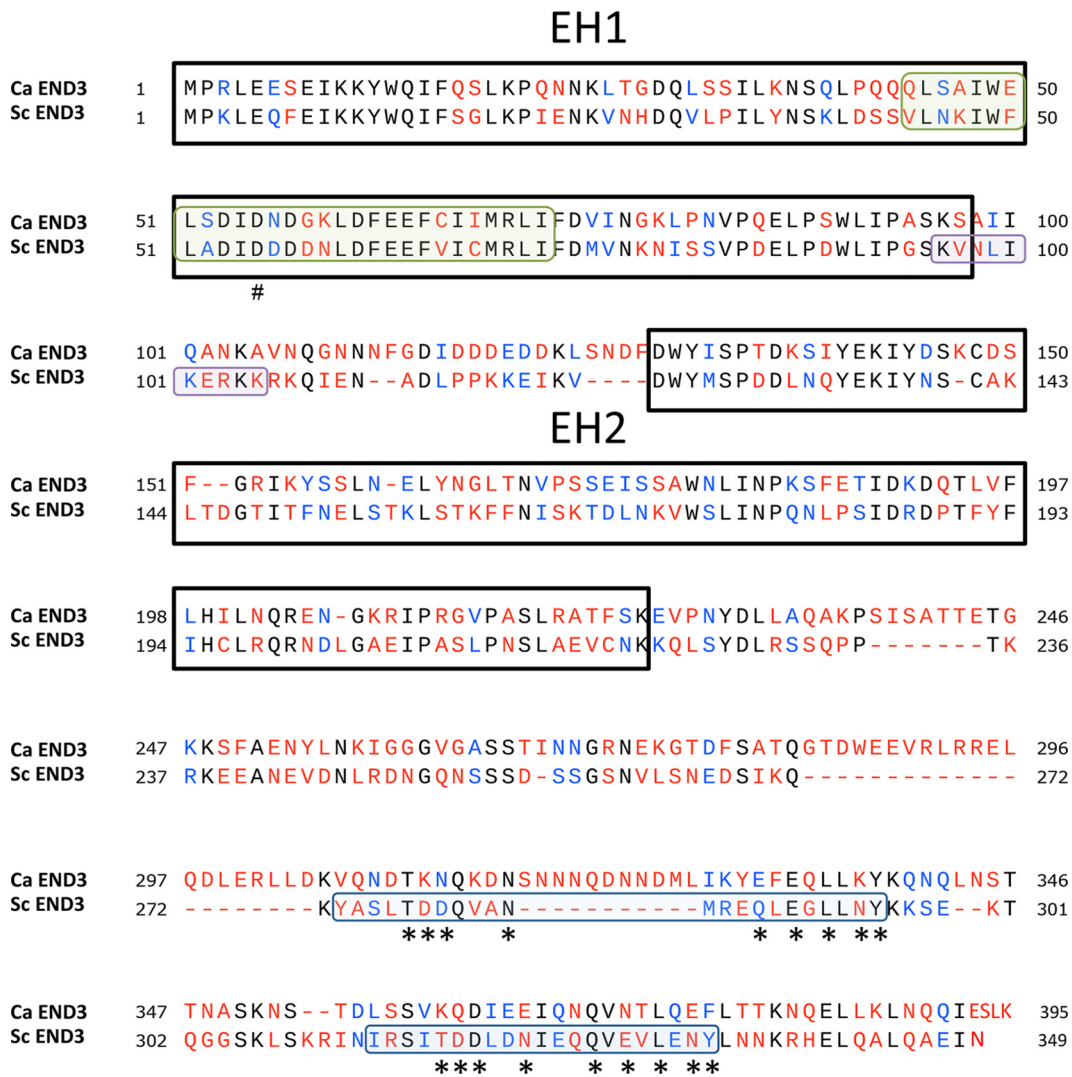
The 40-kDa protein *Sc* End3p plays a central role in the coat assembly process and facilitates the interaction with the actin cytoskeleton during CME (15). *Sc* End3p has two EH domains at the N-terminus that provide a binding site for *Sc* Sla1p (14). The EH1 domain also includes a putative EF-hand Ca(2+)-binding site and part of a consensus sequence for the binding of PIP$_2$ (16). Neither of these two sites are found to be required for End3p function in *Sc* (15). The C-terminal end has a coiled-coil structure known to form a central complex with *Sc* Pal1p and facilitate localization to cortical actin patches and Pan1p phosphorylation (14). The tandem repeats of the coiled-coil region appear to act independently of one another and provide redundant binding sites for Pan1. Mutations of the End3 repeats revealed that the amino acid residues that are conserved between these repeats are the actual binding sites for Pan1p (14). End3p and Pan1p are likely recruited to endocytic sites via interactions with Sla2p and Ent1p. Pan1p has been found to bind Sla2p and Ent1p *in vitro* (10, 17, 18) The Pan1-End3p complex is connected with Sla1p through interactions with the End3 N-terminus (13). End3p plays the crucial role in this recruitment as Pan1p is redundant in this aspect (13, 19).

Even though *Sc* End3p is important for efficient CME based internalization of endocytic vesicles (15), the *end3Δ* mutant is viable and exhibits a normal axial budding pattern, but cytokinesis is inhibited. Calcofluor White (CW) staining of *Sc end3Δ* reveals distorted chitin and cell wall distribution. Cell size and actin organization are altered in the *Sc end3Δ* mutant with fewer cortical actin patches (15). These phenotypic characteristics are tightly linked to complex formation with Pan1p and Sla1p because preventing these interactions, as well as the deletion of any of these genes, results in similar phenotypes (20).

In this study we have characterized the End3 homolog in *Candida albicans* (*Ca*) and have identified similar phenotypes similar to that seen in the *Sc end3* mutant. While endocytosis and cell wall integrity defects were very prominent in the *Ca end3Δ/Δ* deletion strain, cell morphology appeared to be normal. Moreover, the subsequent defects in endocytosis also produce alterations in characteristics specific to *C. albicans* such as filamentation and other virulence-related attributes. Our findings support the concept of existing biological intersections between endocytosis and other secretory pathways.

RESULTS

Structural characterization and identification of *C. albicans END3* as the ortholog of *S. cerevisiae END3*. A search of the *C. albicans* genome database for orthologs of *Sc END3* revealed a 1,188 bp intron-less open reading frame (ORF) (*Ca orf19.1711*) whose deduced protein product is predicted to be a 395-aa protein having overall 36%

EH1

```
Ca END3    1   MPRLEESEIKKYWQIFQSLKPQNNKLTGDQLSSILKNSQLPQQQLSAIWE   50
Sc END3    1   MPKLEQFEIKKYWQIFSGLKPIENKVNHDQVLPILYNSKLDSSVLNKIWF   50

Ca END3   51   LSDIDNDGKLDFEEFCIIMRLIFDVINGKLPNVPQELPSWLIPASKSAII  100
Sc END3   51   LADIDDDDNLDFEEFVICMRLIFDMVNKNISSVPDELPDWLIPGSKVNLI  100
                    #

Ca END3  101   QANKAVNQGNNNFGDIDDDEDDKLSNDFDWYISPTDKSIYEKIYDSKCDS  150
Sc END3  101   KERKKRKQIEN--ADLPPKKEIKV----DWYMSPDDLNQYEKIYNS-CAK  143
```

EH2

```
Ca END3  151   F--GRIKYSSLN-ELYNGLTNVPSSEISSAWNLINPKSFETIDKDQTLVF  197
Sc END3  144   LTDGTITFNELSTKLSTKFFNISKTDLNKVWSLINPQNLPSIDRDPTFYF  193

Ca END3  198   LHILNQREN-GKRIPRGVPASLRATFSKEVPNYDLLAQAKPSISATTETG  246
Sc END3  194   IHCLRQRNDLGAEIPASLPNSLAEVCNKKQLSYDLRSSQPP-------TK  236

Ca END3  247   KKSFAENYLNKIGGGVGASSTINNGRNEKGTDFSATQGTDWEEVRLRREL  296
Sc END3  237   RKEEANEVDNLRDNGQNSSSD-SSGSNVLSNEDSIKQ------------  272

Ca END3  297   QDLERLLDKVQNDTKNQKDNSNNNQDNNDMLIKYEFEQLLKYKQNQLNST  346
Sc END3  272   --------KYASLTDDQVAN----------MREQLEGLLNYKKSE--KT  301
                       ***    *                 *  *  **

Ca END3  347   TNASKNS--TDLSSVKQDIEEIQNQVNTLQEFLTTKNQELLKLNQQIESLK  395
Sc END3  302   QGGSKLSKRINIRSITDDLDNIEQQVEVLENYLNNKRHELQALQAEIN    349
                       ***  *    *  *  **
```

FIG 1 *C. albicans* End3p bears strong homology to *S. cerevisiae* End3p. The alignment of *S. cerevisiae* End3p with *C. albicans* End3p is shown. Identical amino acid residues are shown in black, similar residues in blue, and mismatched residues in red. The black boxes show the conserved epsin homology domains (EH). The green box encloses a putative EFh domain, with the invariant acidic residue marked by the symbol (#). The purple box outlines putative PIP₂ binding domain in *S. cerevisiae* (7). C-terminal coiled coil domains of *Ca* align with *Sc* repeats marked in blue. Asterisks below the *Sc* sequence indicate the residues in *S. cerevisiae* that were found to bind Pan1 (8).

identity and 52% similarity to *Sc* End3p (Fig. 1). The homology is strongest in two regions in the N-terminal region identified by Simple Modular Architecture Research Tool (SMART) (https://smart.embl.de/) as having similarity to the protein-protein interaction modules called epsin homology (EH) domains. Comparing *Ca* and *Sc* End3p, EH domain 1 has 60% identity and 73% similarity, whereas EH2 is less well conserved. The first EH domain also has a weak match to consensus EFhand (EFh), a calcium binding motif found in both *Sc* (15) and *Ca*. These motifs are generally found in pairs and utilize the oxygens of the conserved glutamate or aspartate residues for binding calcium. Only a single EFh is discernible in End3p in either *Ca* or *Sc*. *Sc* also has a putative PIP₂ binding site (15), the sequence of which is partially conserved (50% similarity) in *Ca*.

The carboxyl half of the *Ca* End3p has regions of low complexity and coiled coils, the latter are predicted to be involved with protein-protein interactions. There is some similarity (up to 62% in the second repeat) between the species that align with regions identified in *Sc* as two C-terminal repeats (Fig. 1) shown to be essential for End3p function (15) and involved in binding to Pan1p (14) In *Sc*, the repeats are found to be
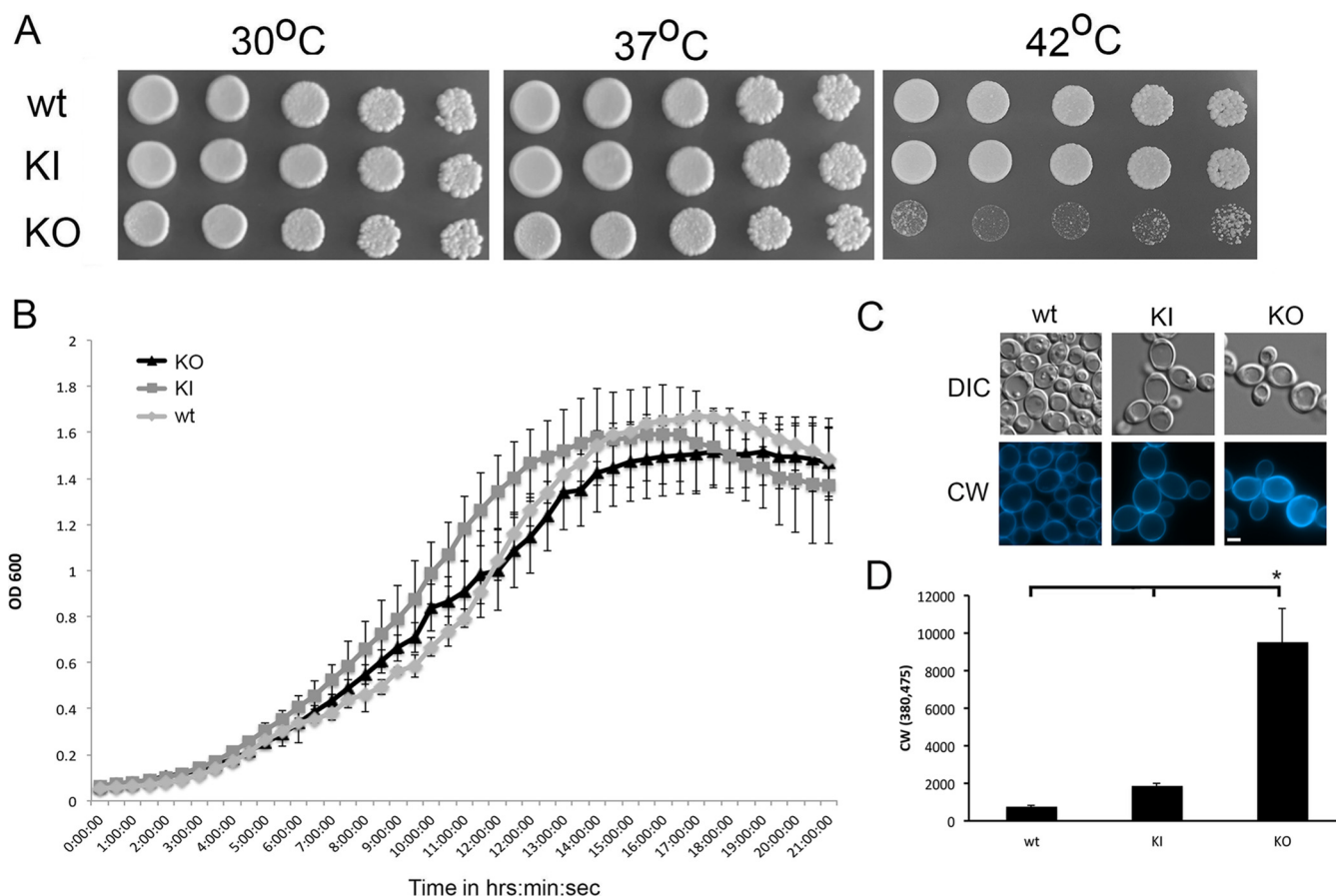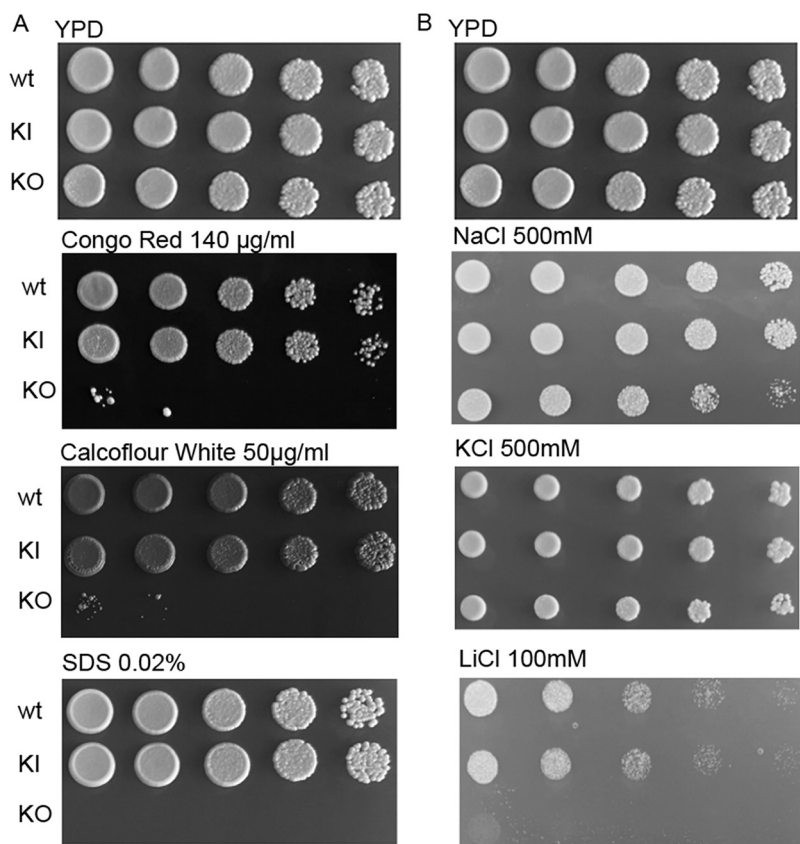
FIG 2 The *end3Δ/Δ* null mutant strain grows comparably to control strains. The *end3Δ/Δ* null mutant strain (KO), wild type (wt), and knock in strain (KI) were depicted on YPD plates incubated for 48 h at (A) 30°C to 42°C, and visualized (B) in a growth curve, (C) by DIC and fluorescence microscopy with Calcofluor White (CW) staining, and (D) in a quantitative analysis for CW staining. The bar is 5 μm. Results shown in (A and C) are a representative of three different experiments. Error bars in (B, D) are the standard deviation of three different data sets. Each individual data point was run in triplicate and was averaged. Statistical significance in (D) between control strains (wt, KI) and KO was determined with the Student's *t* test (wt/ko *P* = 0.0008; KI/KO *P* = 0.001).

redundant with respect to their ability to bind to Pan1p (14). The residues that were identified in *Sc* to participate in binding to Pan1p are only partially conserved in *Ca*.

Construction of a *C. albicans* end3Δ/Δ mutant. To determine the function of *C. albicans END3* we used a reverse genetics approach to analyze gene function. The CRISPR-Cas9 method was used to generate a *C. albicans* end3Δ/Δ null mutant (KO) and corresponding complemented, or "knock-in" (KI) strain, where both copies of the wild-type allele were reintroduced into the *end3Δ/Δ* null mutant (23). Correct strain construction was confirmed by Southern blotting and PCR (sFig.1).

Contribution of *END3* to growth, viability, and cell morphology. The *end3Δ/Δ* null mutant (KO) grows normally compared to wild-type and the complemented control strain (wt, KI; Fig. 2A and B). This finding was confirmed on yeast extract peptone dextrose (YPD) plates (Fig. 2A, 30°C) and in a growth curve in liquid media (Fig. 2B). The doubling times of KO, KI, and wt were 3.6 $\pm$0.24, 3.6 $\pm$0.32 and 3.4 $\pm$0.18 h, respectively. Next, we detected increased temperature sensitivity at 42°C in the KO compared with controls (Fig. 2A). The *end3Δ/Δ* mutant's cell and vacuolar morphology appeared normal when cells were observed via differential interference contrast (DIC) microscopy (Fig. 2C). Cells were stained with CW and visualized using fluorescence microscopy which revealed that the *end3Δ/Δ* null mutant had an enhanced peripheral stain which suggests altered cell wall chitin deposition in the mutant (Fig. 2C and D). These findings indicate that *END3* has a role in cell wall integrity.

Contribution of *END3* to stress tolerance. We next characterized the growth of the *end3Δ/Δ* mutant (KO) in response to cell wall and osmolar stress as well as
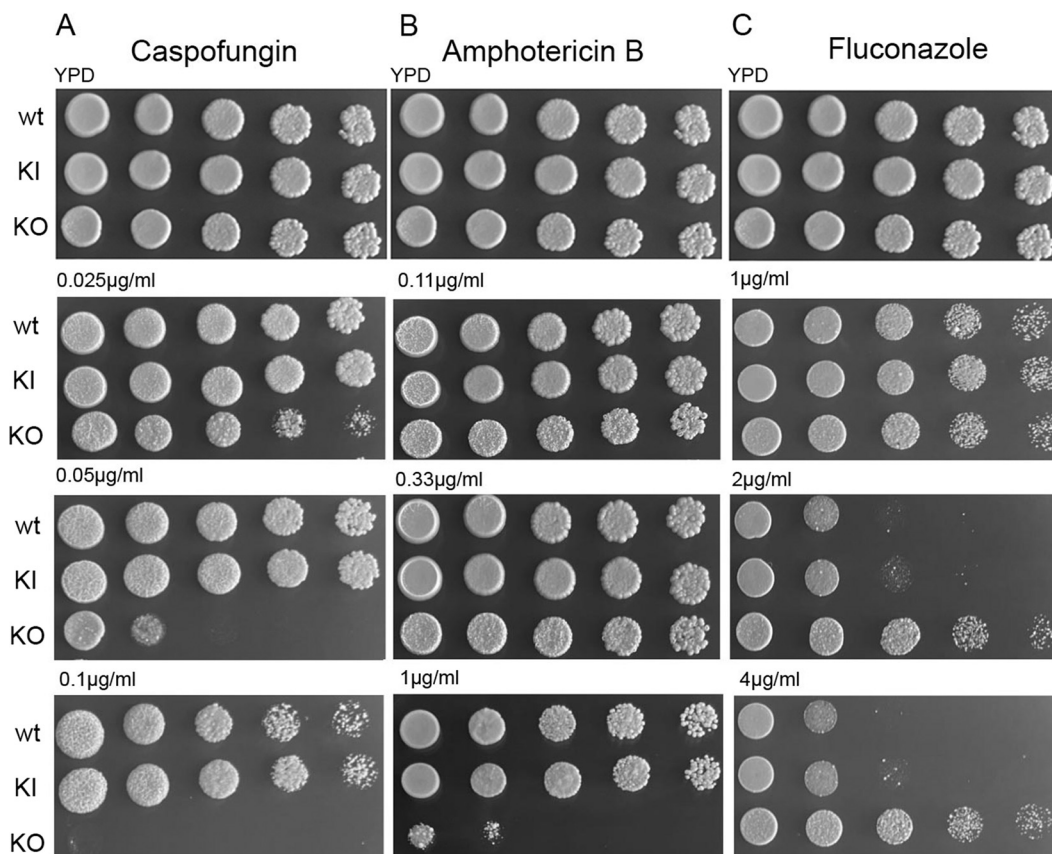
FIG 3 The *end3Δ/Δ* mutant strain has a decreased tolerance to cell wall and ion stress. *end3Δ/Δ* null mutant (KO), wild type (wt), and knock in (KI) strains were grown for 48 h on YPD plates containing (A) cell wall stressors SDS (0.05%), Calcofluor White (50 μg/mL), and Congo red (140 μg/mL), and (B) cationic cell stress conditions including 500 mM KCl, 500 mM NaCl, or 100 mM LiCl. Experiments shown in are a representative of three different experiments.

antifungal agents to characterize the functionality of the cell wall and membrane. When the strains were grown on YPD plates for 48 h at 30°C containing the cell walls stressors SDS (0.05%), CW (50 μg/mL), or Congo red (140 μg/mL), the *C. albicans end3Δ/Δ* mutant demonstrated a dramatic growth defect in comparison to control strains (Fig. 3A). Next, strains were assessed in conditions of high osmolar and/or cation stress (500 mM NaCl, KCl, and 100 mM LiCl) on YPD plates for 48 h at 30°C. In conditions with high NaCl concentrations, the *end3Δ/Δ* mutant grew slower when compared to controls strains, and not at all when exposed to LiCl (Fig. 3B). In contrast, on YPD with high KCl concentrations, there was no growth defect.

We then analyzed growth on plates with YPD media containing antifungal agents to address whether the defects in cell wall integrity and response to osmotic stress correlated with altered sensitivity to antifungal agents. Three commonly used antifungal drugs were selected, fluconazole, caspofungin, and amphotericin B. Fluconazole function requires cellular internalization, while caspofungin and amphotericin B are active directly on the cell wall and membrane, respectively. When grown on YPD plates for 48 h at 30°C containing different concentrations of caspofungin and amphotericin B, the *C. albicans end3Δ/Δ* mutant exhibited a substantial growth defect at all concentrations (0.025 to 0.1 μg/mL) and the highest concentration (1.0 μg/mL) tested, respectively (Fig. 4A and B). Conversely, in the presence of fluconazole, the *end3Δ/Δ* mutant was less sensitive to the drug than wt and KI (Fig. 4C). While control strains exhibited a dramatic growth defect at 2 and 4 μg/mL fluconazole, growth of the KO strain was not affected. The results suggest that a compromised cell wall and membrane renders the KO more vulnerable to caspofungin and amphotericin B. The resistance of the KO to fluconazole may be related to defects in endocytosis and warrants further mechanistic investigation.

FIG 4 The *end3Δ/Δ* mutant strain has increased susceptibility to amphotericin B and caspofungin and reduced susceptibility to fluconazole. The *end3Δ/Δ* null mutant (KO), wild type (wt) and knock in (KI) strains were grown for 48 h on YPD plates containing antifungal drugs (A) amphotericin B at concentrations of 0.11 μg/mL, 0.33 μg/mL, 1.0 μg/mL; (B) caspofungin at concentrations of 0.025 μg/mL, 0.05 μg/mL, 0.1 μg/mL; and (C) fluconazole at concentrations of 1.0 μg/mL, 2.0 μg/mL, 4.0 μg/mL. Experiments shown in (A to C) are a representative of three different experiments.

The *C. albicans end3Δ/Δ* mutant is defective in endocytosis and actin patch formation. In order to define the role of *END3* in *C. albicans* endocytosis, we used the lipophilic fluorescent dye FM4-64 and microscopy, as described in (42) with some modifications. FM4-64 initially binds the plasma membrane and is then actively internalized by clathrin-based endocytosis followed by transport to the vacuole via endocytic intermediates. Mutants with defects in endocytosis exhibit a time delay in FM4-64 endocytosis and therefore staining of the vacuole and other intracellular membranes.

To reduce the binding of FM4-64 in the cell periphery of the *end3Δ/Δ* mutant (KO) during the endocytosis assay, we followed a protocol described in (43) and incubated the cells with FM4-64 on ice. Visualization with fluorescence microscopy demonstrated that the *end3Δ/Δ* mutant strain did not accumulate FM4-64 in the vacuolar membrane compared to control strains (Fig. 5A) under these conditions. We occasionally observed a very bright diffuse signal of FM4-64 that was comparable with the result when cells were incubated on ice, a condition that inhibits endocytosis (Fig. 5A, Fig. S2). Although vacuoles in the *end3Δ/Δ* mutant appeared normal, there was clearly a time delay in vacuolar staining when compared to control strains indicating a marked, but likely not complete, defect in endocytosis. Our quantitative analysis of vacuolar staining confirmed the microscopy data (Fig. 5B).

Because End3p's putative interaction partner Pan1p is a major contributor to actin organization and recruitment during CME we tested whether actin organization is altered in the *end3Δ/Δ* mutant. Rhodamine phalloidin staining revealed fewer actin patches in the *end3Δ/Δ* mutant when compared with controls (Fig. 5C and D). We determined that wild-type (wt) and the reintegrant strain (KI) had an average of
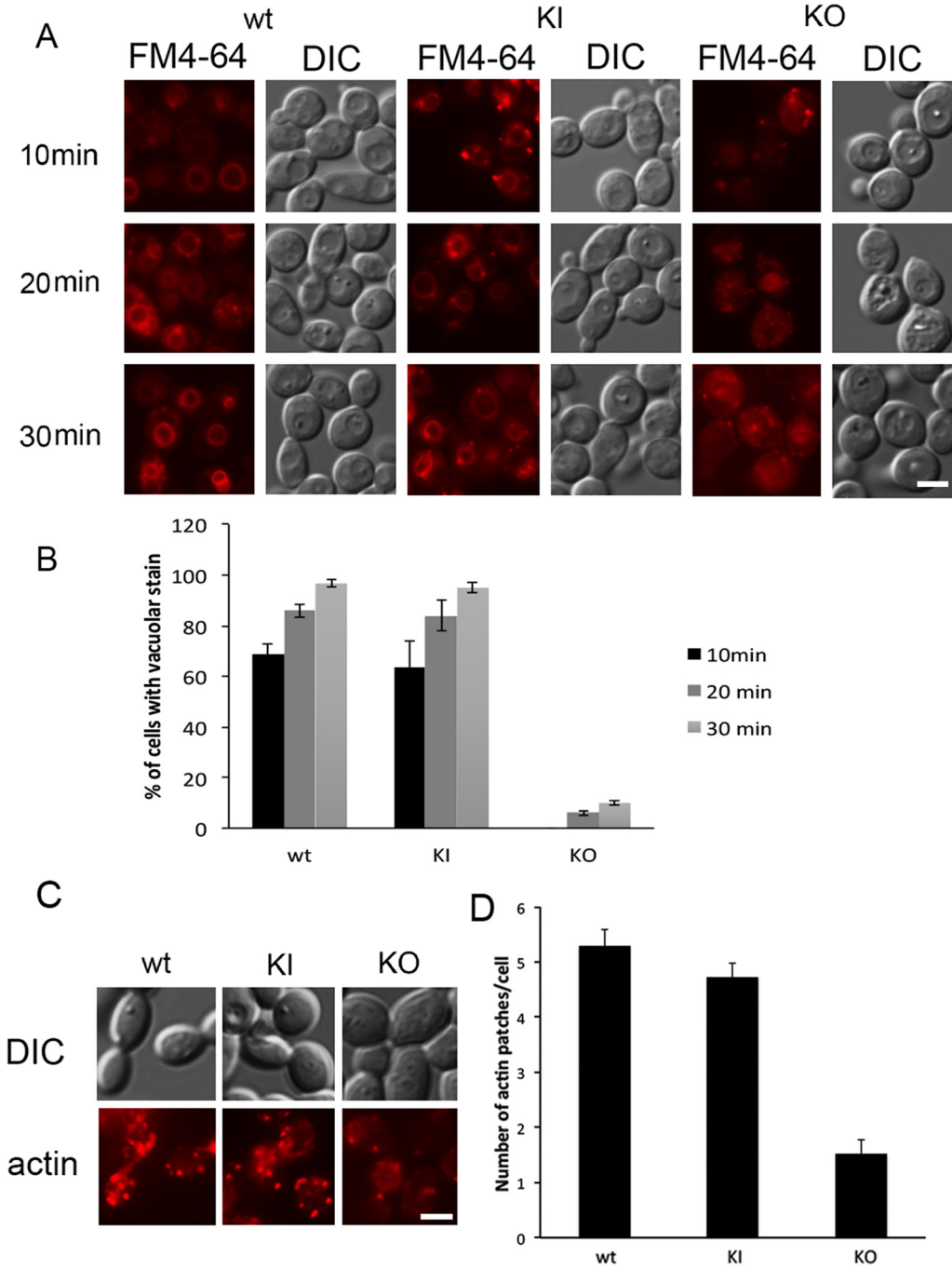
FIG 5 The *end3Δ/Δ* mutant strain has delayed endocytosis and altered actin patch localization. Fluorescent images of the *end3Δ/Δ* null mutant (KO) and control strains, wild type (wt) and knock in (KI) strains stained with the lipophilic fluorescent dye FM4-64 are shown after incubation of 10, 20, and 30 min at RT (A), and with rhodamine-phalloidin to label actin (C). (B) represents a quantitative analysis of cells with vacuolar staining and (D) depicts the statistical analysis of the number of actin patches. Experiments shown in (A) and (C) are a representative of three different experiments. The bars are 5 μm. Error bars in (B) and (D) are the standard deviation of three different experiments. Each individual data point was run in triplicate and was averaged.

5.3 ±0.3 and 4.7 ±0.25 patches/cell, respectively while *end3Δ/Δ* revealed only 1.5 ±0.25 actin patches/cell.

The *C. albicans end3Δ/Δ* mutant is defective in filamentation. Hyphal formation requires efficient endocytosis and a proper cell wall composition. When we tested the ability of the *end3Δ/Δ* mutant to form hyphae compared with controls, the null mutant
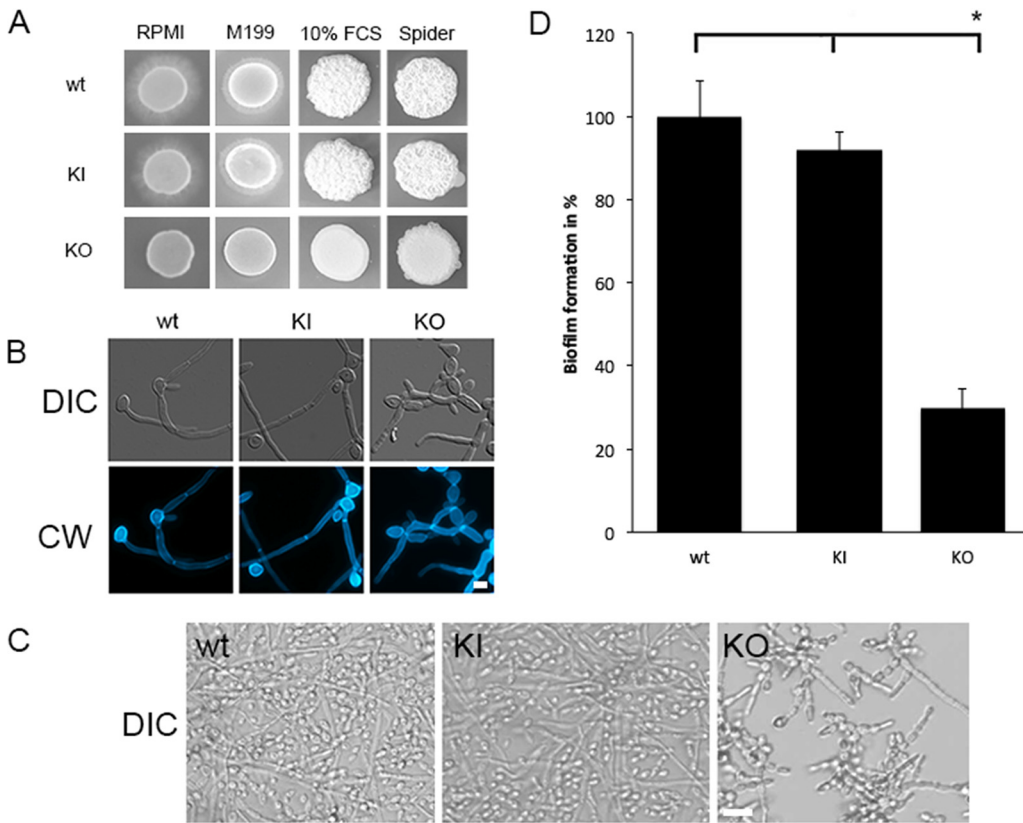
FIG 6 The *end3Δ/Δ* mutant is defective in filamentation and forms an aberrant biofilm. The *end3Δ/Δ* null mutant (KO), wild type (wt) and knock in (KI) strains were assayed (A) on agar plates grown for 72 h at 37°C with different media known to induce hyphal growth. In (B), these strains were grown in liquid RPMI 1640 media overnight and were visualized by DIC and fluorescence microscopy after staining with Calcofluor White. The bar indicates 5 μm. (C) Biofilms were grown on plastic surfaces with RPMI 1640 media for 48 h and assayed for biofilm metabolic activity. (D) These biofilms were visualized by light microscopy using a DIC filter. The bar indicates 50 μm. Experiments shown in (A), (B), and (C) are a representative of three different experiments. Error bars in (D) are the standard deviation of three different data sets. Each individual data point was run in triplicate and was averaged. Statistical significance in (C) between control strains (wt, KI) and KO was determined with the Student's *t* test (wt/KO $P = 0.0002$; KI/KO $P = 0.0002$).

displayed a reduction in filamentation when grown on solid filamentation media such as RPMI 1640 and M199 (Fig. 6A). When the strains were grown on YPD with 10% fetal calf serum (FCS) or Spider medium, some filamentous growth was seen in *end3Δ/Δ* on the edges of the spotted colony similar to controls. When we grew the strains in liquid RPMI 1640 media in strong inducing conditions, we saw a delay in filamentation in the *end3Δ/Δ* mutant, with a predominance of pseudo-hyphal growth while the controls showed true hyphal formation (Fig. 6B).

To test whether the inability to form true hyphae influenced biofilm formation in the *end3Δ/Δ* mutant, we performed detailed studies of biofilm formation using the XTT-reduction assay and light microscopy (Fig. 6C, D). The *end3Δ/Δ* mutant formed a sparse, patchy, poorly adherent biofilm, which lifted easily with minimal disturbance, unlike the wild-type and complemented control (Fig. 6C). Biofilm metabolic activity was reduced by 65% compared with controls (Fig. 6D).

The *C. albicans end3Δ/Δ* mutant is defective in secretion of extracellular proteases. Secretion of conditionally regulated proteins, such as invertase (which is secreted in response to environmental conditions), and trafficking of carboxypeptidase Y to the vacuole is normal in the *S. cerevisiae end3Δ/Δ* mutant (44). However, it is not known whether there are any secretory defects in the *C. albicans end3Δ/Δ* null mutant. Because the Saps are the most extensively studied *C. albicans* secretory proteins (45), we compared the abilities of the *C. albicans end3Δ/Δ* mutant to secrete catalytically-active proteases out of the cell by using bovine serum albumin (BSA) plate assays for
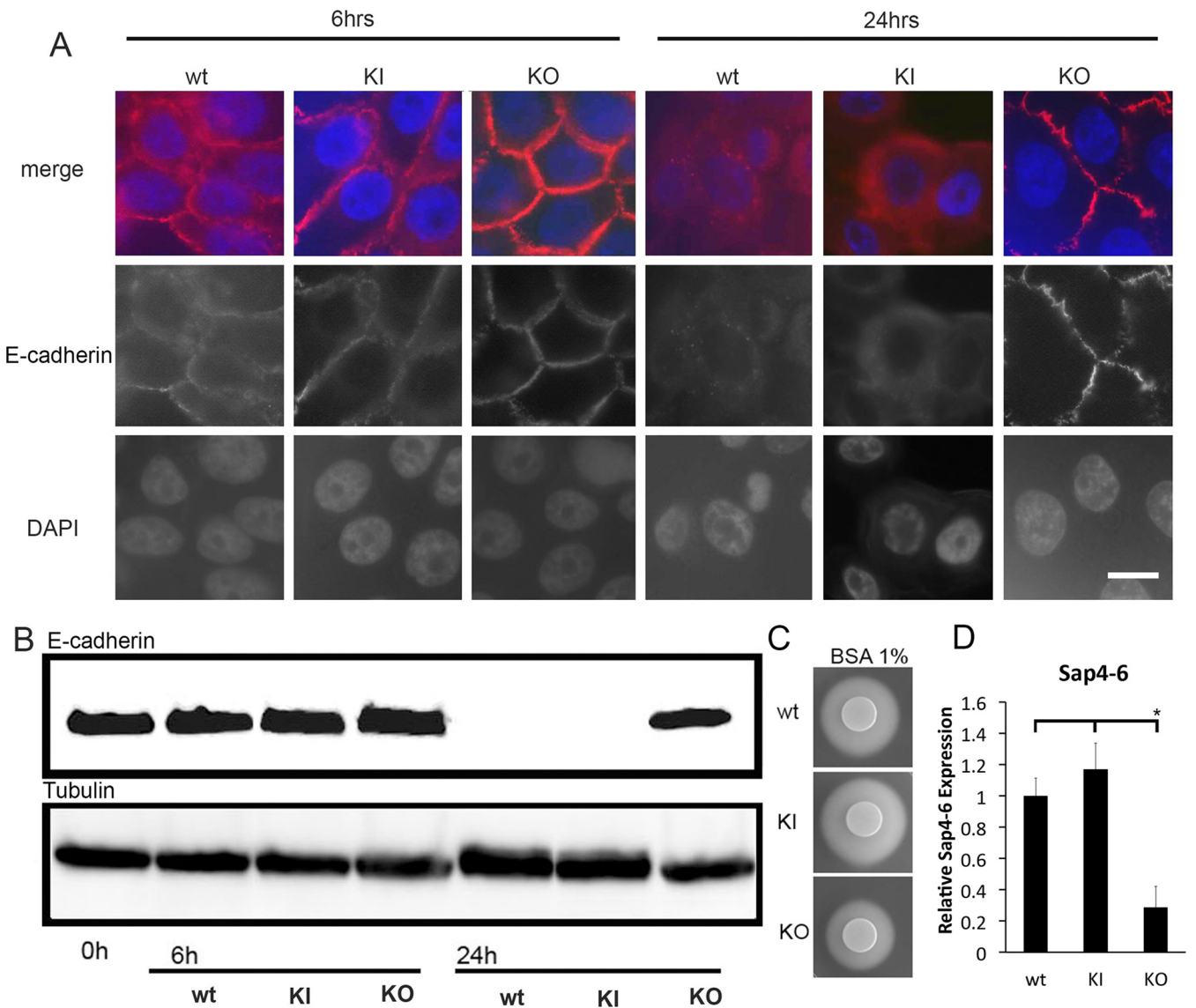
FIG 7 The dissolution of cell–cell adhesions in human VK-2 cells is impaired in the presence of *C. albicans end3Δ/Δ*. Human VK-2 cells infected with the *end3Δ/Δ* null mutant (KO), wild type (wt) and knock in (KI) strains for 6 h and 24 h were visualized (A) by fluorescence microscopy using an antibody against E-Cadherin and DAPI for labeling the nucleus, and (B) were tested by Western blotting for the proteins E-cadherin and Tubulin (loading control). (C) These *C. albicans* strains were further tested in a protease agar plate assay for their ability to lyse BSA after an overnight incubation at 30°C. (D) RNA expression levels of Sap4 to 6 are depicted in *end3Δ/Δ* and control strains after growth in hyphal inducing conditions for 4 h. Experiments shown in (A to D) are a representative of at least three different experiments. The bar in (A) is 10 μm. Statistical significance in (B) between control strains (wt, KI) and KO was determined with the Student's *t* test (wt/KO *P* = 0.014; KI/KO *P* = 0.019).

proteinase secretion. The diameter of an opaque zone around the spotted colony provides an indirect assay of aspartyl protease secretion. In comparison to the control strains (wt, KI), the *end3Δ/Δ* mutant had a smaller zone of BSA degradation. This finding suggests reduced secretion of secreted aspartyl proteases in *end3Δ/Δ* when compared with the controls (Fig. 7C). To further explore this finding, we then assessed the mRNA expression level of Sap4 to 6 in the *end3Δ/Δ* mutant and the control strains under conditions of hyphal growth. Our findings revealed a marked decrease of Sap4 to 6 mRNA expression in the null mutant when compared with wt and KI suggesting that *END3* contributes to secretion of Sap4 to 6.

Dissolution of cell–cell adhesions is impaired in the *C. albicans end3Δ/Δ* mutant. The destruction of tight junctions between host cells is a hallmark of *C. albicans* virulence and is facilitated by the proteases Sap4 to 6 degrading the adhesion molecule E-cadherin (46, 47). To assess the capacity of the *end3Δ/Δ* mutant to compromise tight
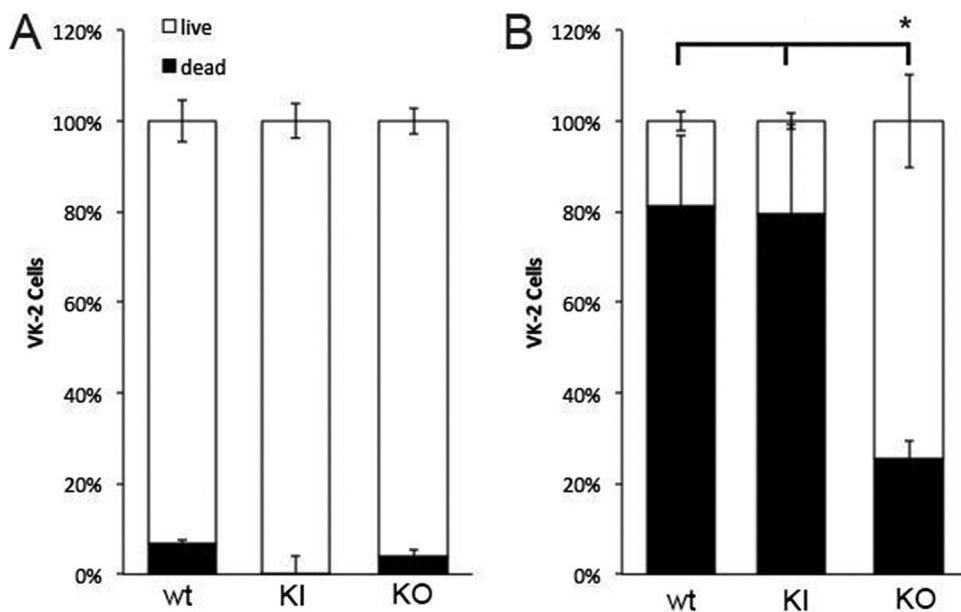
FIG 8 The *C. albicans end3Δ/Δ* mutant has a reduced ability to kill human VK-2 cells *in vitro*. VK-2 cells infected with the *end3Δ/Δ* null mutant (KO), wild type (wt), and knock in (KI) strains for (A) 6 h and (B) 24 h were tested in a LIVE/DEAD assay. Error bars in (A) and (B) are the standard deviation of three different data sets. Each individual data point was run in triplicate and was averaged. Statistical significance between control strains (wt, KI) and KO was determined with the Student's *t* test (wt/KO *P* = 0.0003; KI/KO *P* = 0.0003).

junctions, we infected the vaginal human keratinocyte cell line VK-2 with KO and the control strains (wt, KI) for 6 h and 24 h, and evaluated the cells over time for the presence of E-cadherin. Co-culture with *C. albicans* KO, wt, or KI after 6 h of incubation revealed E-cadherin labeled puncta at tight junctions between VK-2 cells. After 24 h, no staining was observed using the anti-E-cadherin antibody in VK-2 cells cocultured with wt and KI (Fig. 7A). In contrast, in VK2-cells exposed to the KO strain, the E-cadherin labeled tight junctions remained intact (Fig. 7A).

The presence of E-cadherin in VK-2 cells during coculture with *C. albicans* was analyzed by Western blotting (Fig. 7B). While at 6 h of incubation, E-cadherin levels were similar between cocultures, by 24 h, E-cadherin was undetectable in cells cocultured with wt and KI strains. In contrast, the E-cadherin level remained stable over time in VK-2 cells incubated with the KO strain (Fig. 7B).

Taken together, these findings suggest reduced secreted protease activity in the *end3Δ/Δ* mutant when compared with control strains, resulting in decreased virulence in this *in vitro* model, as measured by the ability to disrupt cell–cell adhesion of vaginal keratinocytes.

The *C. albicans end3Δ/Δ* mutant lacks the ability to kill host cells. To define the ability of the *end3Δ/Δ* strain to compromise host cell viability, we tested the strain in a host cell killing assay. Using a microplate Live/Dead assay (Invitrogen, Waltham, MA) as described in (28), we evaluated human VK-2 cell growth after 6 h and 24 h of infection with the *end3Δ/Δ* mutant and the control strains KI and wt. After 6 h of infection, 95% of VK-2 cells were alive in cultures with KO and the control strains (Fig. 8A). After 24 h, the KO killed about 25% of VK-2 cells, while wt and KI strains destroyed 80% of host cells (Fig. 8B). This finding underscores the substantially reduced virulence of the *end3Δ/Δ* strain, when assayed *in vitro*.

DISCUSSION

In prior work on secretion in *C. albicans*, we noted that several pre-vacuolar and other secretory mutants had defects not only in exocytic pathways (2, 24, 25, 48, 49), but also appeared to have defects in endocytosis as well (46, 47). These findings

suggested an intersection between these secretory pathways. To further understand this interconnection, we have now turned our focus to analyzing key components of clathrin-based endocytosis, a pathway that remains under-studied in *C. albicans*. A few genes involved in endocytosis such as *EDE1*, *SLA2*, and *SLA1* have been characterized in *C. albicans*, and we have recently analyzed the early endocytosis gene *ENT2* (28). Null mutants of *Ca SLA2*, *SLA1*, and *ENT2* are defective in clathrin-mediated endocytosis whereas the null mutant of *Ca EDE1* does not appear to have this defect (50).

Here we have identified *Ca END3* to be a non-essential gene. The corresponding null mutant is defective in efficient endocytosis and actin patch formation. While this finding is consistent with the (*Sc*) *end3*Δ null mutant there are some substantial morphological and growth differences. Unlike in the *Sc end3*Δ mutant, we were unable to identify a bipolar budding pattern, an abnormal enlarged cell shape, and altered vacuolar morphology in the *Ca end3*Δ/Δ mutant. On the other hand, the null mutant of the putative End3p binding partner Sla1p, has a reduced growth rate and forms enlarged, globular mother cells due to delays in cell cycle progression. Our recent studies of the null mutant of *Ca ENT2*, which encodes another potential interacting partner of End3p, revealed a slight growth defect but a normal cell shape and vacuolar morphology of the yeast form. These variations are likely a result of different functions in CME.

Consistent with *Sc*, the *Ca end3*Δ/Δ mutant has a strong defect in cell wall morphology and function (15). We observed substantial impairments in cell wall integrity when challenged by a variety of cell wall stressors and antifungal agents that impact the cell wall directly (caspofungin, amphotericin B; Fig. 5A and B). We also detected increased peripheral staining in the *end3*Δ/Δ mutant using dyes such as CW and FM4 to 64 (Fig. 2 and 5A, B, respectively). Because CW binds chitin, this result suggests that there is increased chitin content of the cell wall, potentially as a compensatory response to other defects in cell wall composition or architecture. Why enhanced initial binding of FM4-64, which attaches via membrane insertion, was detected on the cell surface of the *end3*Δ/Δ mutant is not clear and warrants further investigation.

In *Sc*, the Pan1-End3p complex binds to Sla2p and Ent1/2p which couples the complex to the clathrin coat. Consistent with this, we identified phenotypic similarities between the *Ca end3*Δ/Δ and *Ca ent2*Δ/Δ mutants regarding cell wall integrity, hyphal formation, and endocytosis defects. Another group has found that the *Ca sla2*Δ/Δ mutant is defective in all polarized secretion including CME and shows mislocalization of lipid rafts that are usually found at the hyphal tip. They further identified mislocalization of Rvs167p, a lipid raft-associated protein, and the cell wall remodeling enzyme Gsc1p, which is a b-1,3-glucan synthase (51). The actin binding Arp2/3 complex that interacts with the PaII-End3p complex is also required for cell wall integrity (38). These findings suggest that defects in cell wall integrity may be a common feature in endocytosis mutants.

Improperly functioning endocytic transport in the *end3*Δ/Δ mutant has consequences for the secretion of extracellular components. As *C. albicans* proteases Sap4 to 6 are responsible for degrading E-cadherin in host cells (52), the inability of the *end3*Δ/Δ mutant to break down E-cadherin in a vaginal epithelial cell line, and reduced extracellular BSA degradation (Fig. 7A to C) suggests that their secretion is reduced in the *end3*Δ/Δ strain. Our studies of *Ca ent2*Δ/Δ revealed a deficiency in secretion of extracellular proteases as well. These findings provide direct and indirect evidence for impairments in cellular trafficking other than endocytosis and suggest intersection of these pathways.

We also found that the *end3*Δ/Δ mutant is impaired in proper hyphal formation and only produced a weak biofilm (Fig. A to D), which is likely related to the dramatic changes of the cell wall and the need for massive secretion of extracellular components during these processes. The *end3*Δ/Δ mutant in strong hyphal-inducing conditions had a predominantly pseudo-hyphal appearance. Similar findings were seen in binding partners of End3p. For instance, the *Ca sla1*Δ/Δ mutant produced shorter filaments in hyphal-inducing conditions (37) and the *Ca ent2*Δ/Δ mutant was unable to form hyphae and biofilms all together (28). Interestingly, while the *Ca* actin-binding Arp2/3p complex is required for hyphal and biofilm formation it does not have an essential function for endocytosis (38, 39).

TABLE 1 Strain table

Name	Description/ genotype	Reference
AHY940	SC5314 *LEU2* heterozygous knockout a/α *leu2Δ/LEU2*	(23)
CREnd3KO	SC5314 end3 homozygous knockout a/α *end3Δ/end3Δ*	This study
CREnd32KI	SC5314 *end3* homozygous knock in a/α *end3Δ/end3Δ END3/END3*	This study

The impaired hyphal growth, cell wall integrity, and transport defects in the *end3Δ/Δ* mutant were associated with a greatly reduced virulence-related phenotypes in our *in vitro* assays. The Live/Dead assay revealed only a limited ability of the *end3Δ/Δ* mutant to kill host cells, a characteristic that was found in *Ca ent2Δ/Δ* as well (28). The pseudo-hyphal growth and the limited ability to secrete proteases that degrade host cell E-cad-herin provide a mechanistic explanation for this greatly reduced ability to damage host cells in this *in vitro* model.

Our study suggests that *C. albicans* End3p provides a connection between endocytosis and other intracellular transport pathways, as well as a contribution to cell wall integrity and hyphal formation. It demonstrates that an impairment in endocytosis leads to serious implications for cell function and virulence-related properties in *C. albicans*. These roles are partially shared with the late coat proteins, Ent2p and Sla1p, suggesting that late coat assembly is central for a functional endocytic process. Further investigations of the role of CME in virulence including *in vivo* studies, are therefore warranted.

MATERIALS AND METHODS

Identification of *C. albicans* END3. The predicted protein and DNA sequences for *Sc* and *Ca END3* were retrieved from the Saccharomyces Genome Database (http://www.yeastgenome.org) and Candida Genome Database (http://www.candidagenome.org), respectively. A single potential ortholog to *Sc* End3p was identified by a BLASTp search of the Candida Genome Database utilizing the functions on these websites. Alignments of the protein sequences was done with the SnapGene (SnapGene.com) protein align function, using the Smith-Waterman method (21). The web resource, SMART, available at https://smart.embl.de, (22) was utilized for the identification and annotation of protein domains.

Deletion of *C. albicans* END3 and Southern blotting. Table 1 includes the list of oligonucleotides and primers used for gene deletion and Southern blotting experiments. We generated a *C. albicans end3Δ/Δ* null mutant using the CRISPR-Cas9 protocol developed by the Hernday laboratory (23). Alleles of *END3* were then re-integrated via homologous recombination into the *end3Δ/Δ* null mutant to gener-ate a complemented KI strain. Correct strain construction was demonstrated by Southern blotting. Briefly, 5 μg genomic DNA was digested with SphI and SpeI overnight and loaded onto a 1% agarose gel. The blot was performed using standard protocols. A DNA probe was generated by PCR using DIG-la-beled dNTP (Roche, Basel, Switzerland). Detection of the probe was visualized with a DIG Luminescent Detection Kit (Roche, Basel, Switzerland).

Preparation of genomic DNA and plasmid isolation. Genomic DNA was extracted from yeast cells using the MasterPure Yeast DNA purification kit (Epicentre Biotechnologies, Madison, WI) following to manu-facturer's instructions. Competent *Escherichia coli* DH5α cells (Invitrogen, Waltham, MA) were used to gener-ate and maintain plasmids. *E. coli* cells carrying plasmids of interest were grown in LB medium (1% tryptone, 0.5% glucose, and 1% NaCl) with 100 μg/mL ampicillin at 37°C. Plasmid DNA was extracted from overnight cultures using the Qiagen Plasmid Miniprep system (Qiagen, Germantown, MD) according to the manufac-turer's instructions. Plasmids used and generated in this study are listed in Table 2.

Strains, media, and cell culture. The *C. albicans* strains utilized in this study are listed in Table 3. YPD (1% yeast extract, 2% peptone, 2% glucose) or (yeast nitrogen base [YNB], 6.7g, plus amino acids, and 2% glucose) were used as a standard growth media. Unless otherwise stated, liquid cell cultures were established by incubation at 30°C with shaking at 250 rpm.

VK-2/E6E7 (ATCC CRL-2616, Manassas, VA), a human vaginal keratinocyte cell line, was grown in Keratinocyte-SFM media (Invitrogen, Waltham, MA) in a cell culture incubator at 37°C with 5% CO_2. Following the manufacturer's instructions, cells were split once a week and fed every 2 days.

Cell growth assay and agar plate assays for response to environmental stress and filamentation. To assay growth curves, cells from an overnight culture in YPD at 30°C were counted and diluted in YPD to a cell concentration of 1×10^6 cells/mL. Then, 100 μL of this cell dilution were placed in 96-well plates, in quadruplicate. Cell growth was determined over 21 h at 30°C using a microplate reader (BioTek Synergy H1, Winooski, VT) that recorded the extinction at OD 600 nm every 30 min.

Growth rates were assessed on agar plate assays as described (24, 25). Five μL of cells from 1:5 serial dilutions were spotted onto agar plates. Growth was assayed after 48 h in response to 30°C, 37°C, and 42°C, cell wall stressors (0.2% SDS in YPD, 140 μg/mL Congo red in YNB, 50 μg/mL CW in YNB, all from Sigma-Aldrich, St. Louis, MO), potassium chloride, lithium chloride, and sodium chloride (all Sigma-Aldrich, St. Louis, MO) in YPD, BSA with YNB (26) as well as antifungal drugs (amphotericin B,

TABLE 2 Plasmids

Name	Description	Reference
pADH137	C.alb LEUpOUT CAS9 expression plasmid	(23)
pADH118	C.alb LEUpOUT "blank" gRNA plasmid	(23)
pCREnt2	C.alb LEUpOUT "blank" gRNA plasmid with End3 guide RNA	This study

caspofungin, fluconazole, all Sigma-Aldrich, St. Louis, MO, in YPD). Filamentation was determined after 72 h at 37°C on solid YPD with 10% (vol/vol) fetal calf serum (FCS, Fisher Scientific, Waltham, MA), Medium 199 supplemented with L-glutamine (M199, Sigma-Aldrich, St. Louis, MO), RPMI 1640 pH 7.0 (Fisher Scientific, Waltham, MA), and Spider medium, as described previously (27).

Analyses of endocytosis and fluorescence-activated cell sorting with FM4-64. The lipophilic membrane dye FM4-64 [N-(3-triethylammoniumpropyl)-4-(6-(4-(diethylamino)phenylhexatrienyl) pyridiniumdibromide] (EMD Millipore, Temecula, CA), which is actively endocytosed, was used to assay membrane-related endocytosis as described (28). Briefly, FM4-64 at a final concentration of 2 mM was added and incubated on ice for 20 min to ice cold strains that have been grown to a mid-log phase. The cells were washed in ice cold PBS and were incubated at room temperature for 10, 20, and 30 min. Membrane transport at each time point was stopped with ice cold 12 mM sodium azide (Sigma-Aldrich, St. Louis, MO). Staining of the vacuoles was visualized using a Zeiss Axio Imager M1 fluorescence microscope. Images were taken using standard Texas Red filters for FM4-64 and analyzed for the ability to stain the vacuolar membrane.

Actin staining. Strains were grown to exponential phase in YPD and fixed in 3% paraformaldehyde (Sigma-Aldrich, St. Louis, MO) for 90 min. Actin staining was performed with rhodamine phalloidin after permeabilization with Triton X-100 using the protocol described in (29). For the analysis, the number of actin patches of each individual cell was counted in approximately 100 cells per strain. The total number of actin patches was determined and averaged by the counted cell number. The standard deviation was calculated from the average of the three experiments for each strain.

Analysis of adherence and biofilm formation in *C. albicans* endocytosis mutants. Biofilms were visualized via DIC light microscopy on a Nikon Eclipse Ti inverted microscope, and metabolic activity was measured by XTT-reduction, in triplicate, according to published methods (30). Briefly, the XTT-reduction assay was performed after 48 h of biofilm growth at 37°C. Films were washed and incubated with the XTT-menadione substrate at 37°C for 3 h. Supernatant was transferred to a fresh 96-well plate, and absorbance was read at 490 nm in a microplate reader (BioTek Synergy H1, Winooski, VT). Experiments were performed in triplicate, each with eight replicates per strain. Statistical significance was assessed using the Student's *t* test in Microsoft Excel.

Immunofluorescence microscopy of *C. albicans* strains. Cell morphology of yeast and hyphal forms was assessed via fluorescence microscopy as described (28, 31). Cells from an overnight culture in YPD at 30°C (yeast growth) or 37°C in RPMI 1640 (filamentous growth) were mixed 20:1 with CW (Sigma-Aldrich, St. Louis, MO), placed on a slide and visualized with a 63× lens and DAPI filter of a Nikon Eclipse 80i microscope.

Quantitative plate assay of *C. albicans* strains CW staining. For the quantitative plate assay, 1.0×10^6 cells from each strain were mixed 20:1 with CW and incubated for 30 min. Cells were washed six times with ice cold PBS, resuspended in 300 μL and placed in triplicates of 100 μL solutions into 96-well

TABLE 3 Primer

Name	Sequence	Reference
Hu EcadherintandF	gtc tgt agg aag gca cag cc	(40)
Hu EcadherintndR	tgc aac gtc gtt acg agt ca	(40)
Hu GAPDHF	gga cct gac ctg ccg tct a	(41)
Hu GAPDHR	tgc tgt agc caa att cgt tg	(41)
End3 inner F	cca atg tcc cac aag aat tac c	This study
End3 inner R	ttg atg gtt ttg ctt gag cc	This study
End3 outer F/donor KI	ata aag gtc gtg tgc ttt gtg t	This study
End3 outer R/donor KI	gtt ctg gat gtt act gct ga	This study
End3 probe Southern F	gac tca ctt act tgc cgc ct	This study
End3 probe Southern R	cgt gac ta caca cag cac acg	This study
End3 KO donor U.90	aat tat tta tac atc ttc gtc tct tcc cta ttt acg aaa aat gcg aat ttt taa atc caa aga atc aag aat tat taa aat taa atc aac	This study
End3 KO donor L.90	gtt gat tta att tta ata att ctt gat tct ttg tag tta aaa att cgc att ttt cgt aaa tag gga aga gac gaa gat gta taa ata att	This study
End3 guide RNA oligo	cgt aaa cta ttt tta att tga ttt ctg att ctt cta aac ggt ttt aga gct aga aat agc	This study
AHO1098	caaattaaaaatagtttacgcaag	(23)
AHO1099	gtt tta gag cta gaa atg caa gtt	(23)

plates. The strains were analyzed with a microplate reader (BioTek Synergy H1, Winooski, VT) using excitation and emission filter for CW (380 nm and 475 nm, respectively) and graphed using Microsoft Excel.

Immunofluorescence microscopy of Co-cultured VK-2 cells *with C. albicans* strains. VK-2 cells growing on glass coverslips were infected with *C. albicans end3*Δ/Δ or control strains for 6 h and 24 h in keratinocyte SFM media at 37°C and 5% CO_2 as described (28, 32). The MOI was 0.01 for *C. albicans* strains in these experiments. VK-2 cells were then stained for 1 h with a 1:100 dilution of a E-cadherin primary antibody (R&D, Minneapolis, MN) in 0.2% gelatin PBS then washed and incubated with an anti-mouse-GFP secondary antibody (Invitrogen, Waltham, MA) for another hour. Cover slides were mounted on slides with an antifade mounting solution containing DAPI. A Zeiss Axio Imager M1 microscope was used to visualize the cells using standard GFP and 4′,6-diamidino-2-phenylindole (DAPI) filters.

RNA extraction, reverse transcription, and real-time qPCR. From an overnight culture in YPD, *C. albicans* strains were diluted 1:50 in SFM media and grown for 4 h at 37°C. Cells were harvested and RNA was isolated using the RNeasy-Plus kit (Qiagen, Germantown, MD). A reverse transcription reaction from 100 ng RNA was performed with SuperScript III Reverse Transcriptase according to the manufacturer's instructions (Invitrogen, Waltham, MA). In addition, 1 μL of this reaction was used as a template for a 20 μL real-time qPCR with a Sso Advanced Universal SYBR Green Supermix (Bio-Rad, Hercules, CA) and primers for actin (33) and Sap4 to 6 (34, 35) as described. Reactions were set up in triplicates for each strain and amplified gene.

Western blotting and detection of E-cadherin. Western blotting was performed with a standard protocol as described in (36). Protein lysate was used from VK-2 cells infected with the *C. albicans end3*Δ/Δ mutant or control strains for 6 h and 24 h in keratinocyte SFM media at 37°C and 5% CO_2. Primary antibodies to E-cadherin (R&D systems, Minneapolis, MN) and tubulin (Invitrogen, Waltham, MA) were incubated overnight and were used at 1:500 and 1:1,000 dilutions, respectively. Anti-mouse secondary antibody (Invitrogen, Waltham, MA) was incubated for 1 h in a 1:10,000 dilution. Tubulin was used as a loading control.

Live/Dead viability assay. VK-2 cells were grown in 96-well plates in a serum-free SFM Media to a 30% confluence. *C. albicans* strains were grown overnight in a YPD and were cocultured with VK-2 cells at a concentration of 5×10^5 cell/mL for 6 h and 24 h. The Live/Dead viability assay from Invitrogen (Waltham, MA) was performed using the protocol provided by the manufacturer and as described previously (28). The resulting data were analyzed according to the manufacturer's instructions using Excel (Microsoft).

SUPPLEMENTAL MATERIAL

Supplemental material is available online only.

SUPPLEMENTAL FILE 1, PDF file, 1.1 MB.

REFERENCES

1. Goode BL, Eskin JA, Wendland B. 2015. Actin and endocytosis in budding yeast. Genetics 199:315–358. https://doi.org/10.1534/genetics.112.145540.
2. Rollenhagen C, Mamtani S, Ma D, Dixit R, Eszterhas S, Lee SA. 2020. The role of secretory pathways in *Candida albicans* pathogenesis. JoF 6:26. https://doi.org/10.3390/jof6010026.
3. Brach T, Godlee C, Moeller-Hansen I, Boeke D, Kaksonen M. 2014. The initiation of clathrin-mediated endocytosis is mechanistically highly flexible. Curr Biol 24:548–554. https://doi.org/10.1016/j.cub.2014.01.048.
4. Mooren OL, Galletta BJ, Cooper JA. 2012. Roles for actin assembly in endocytosis. Annu Rev Biochem 81:661–686. https://doi.org/10.1146/annurev-biochem-060910-094416.
5. Lu R, Drubin DG. 2017. Selection and stabilization of endocytic sites by Ede1, a yeast functional homologue of human Eps15. Mol Biol Cell 28:567–575. https://doi.org/10.1091/mbc.E16-06-0391.
6. Stimpson HEM, Toret CP, Cheng AT, Pauly BS, Drubin DG. 2009. Early-arriving Syp1p and Ede1p function in endocytic site placement and formation in budding yeast. Mol Biol Cell 20:4640–4651. https://doi.org/10.1091/mbc.e09-05-0429.
7. Wendland B, Steece KE, Emr SD. 1999. Yeast epsins contain an essential N-terminal ENTH domain, bind clathrin and are required for endocytosis. EMBO J 18:4383–4393. https://doi.org/10.1093/emboj/18.16.4383.
8. Yamamoto W, Wada S, Nagano M, Aoshima K, Siekhaus DE, Toshima JY, Toshima J. 2018. Distinct roles for plasma membrane PtdIns(4)P and PtdIns(4,5)P2 during receptor-mediated endocytosis in yeast. J Cell Sci 131.
9. Aguilar RC, Longhi SA, Shaw JD, Yeh L-Y, Kim S, Schön A, Freire E, Hsu A, McCormick WK, Watson HA, Wendland B. 2006. Epsin N-terminal

homology domains perform an essential function regulating Cdc42 through binding Cdc42 GTPase-activating proteins. Proc Natl Acad Sci U S A 103:4116–4121. https://doi.org/10.1073/pnas.0510513103.
10. Wendland B, Emr SD. 1998. Pan1p, yeast eps15, functions as a multivalent adaptor that coordinates protein-protein interactions essential for endocytosis. J Cell Biol 141:71–84. https://doi.org/10.1083/jcb.141.1.71.
11. Feliciano D, Di Pietro SM. 2012. SLAC, a complex between Sla1 and Las17, regulates actin polymerization during clathrin-mediated endocytosis. Mol Biol Cell 23:4256–4272. https://doi.org/10.1091/mbc.E11-12-1022.
12. Tang HY, Cai M. 1996. The EH-domain-containing protein Pan1 is required for normal organization of the actin cytoskeleton in *Saccharomyces cerevisiae*. Mol Cell Biol 16:4897–4914. https://doi.org/10.1128/MCB.16.9.4897.
13. Sun Y, Leong NT, Wong T, Drubin DG. 2015. A Pan1/End3/Sla1 complex links Arp2/3-mediated actin assembly to sites of clathrin-mediated endocytosis. Mol Biol Cell 26:3841–3856. https://doi.org/10.1091/mbc.E15-04-0252.
14. Whitworth K, Bradford MK, Camara N, Wendland B. 2014. Targeted disruption of an EH-domain protein endocytic complex, Pan1-End3. Traffic 15:43–59. https://doi.org/10.1111/tra.12125.
15. Bénédetti H, Raths S, Crausaz F, Riezman H. 1994. The *END3* gene encodes a protein that is required for the internalization step of endocytosis and for actin cytoskeleton organization in yeast. Mol Biol Cell 5:1023–1037. https://doi.org/10.1091/mbc.5.9.1023.
16. Riezman H. 1985. Endocytosis in yeast: several of the yeast secretory mutants are defective in endocytosis. Cell 40:1001–1009. https://doi.org/10.1016/0092-8674(85)90360-5.

17. Toshima J, Toshima JY, Duncan MC, Cope MJTV, Sun Y, Martin AC, Anderson S, Yates JR, Mizuno K, Drubin DG. 2007. Negative regulation of yeast Eps15-like Arp2/3 complex activator, Pan1p, by the Hip1R-related protein, Sla2p, during endocytosis. Mol Biol Cell 18:658–668. https://doi.org/10.1091/mbc.e06-09-0788.

18. Boeke D, Trautmann S, Meurer M, Wachsmuth M, Godlee C, Knop M, Kaksonen M. 2014. Quantification of cytosolic interactions identifies Ede1 oligomers as key organizers of endocytosis. Mol Syst Biol 10:756. https://doi.org/10.15252/msb.20145422.

19. Warren DT, Andrews PD, Gourlay CW, Ayscough KR. 2002. Sla1p couples the yeast endocytic machinery to proteins regulating actin dynamics. J Cell Sci 115:1703–1715. https://doi.org/10.1242/jcs.115.8.1703.

20. Tang HY, Xu J, Cai M. 2000. Pan1p, End3p, and S1a1p, three yeast proteins required for normal cortical actin cytoskeleton organization, associate with each other and play essential roles in cell wall morphogenesis. Mol Cell Biol 20:12–25. https://doi.org/10.1128/MCB.20.1.12-25.2000.

21. Smith TF, Waterman MS. 1981. Identification of common molecular subsequences. J Mol Biol 147:195–197. https://doi.org/10.1016/0022-2836(81)90087-5.

22. Schultz J, Milpetz F, Bork P, Ponting CP. 1998. SMART, a simple modular architecture research tool: identification of signaling domains. Proc Natl Acad Sci U S A 95:5857–5864. https://doi.org/10.1073/pnas.95.11.5857.

23. Nguyen N, Quail MMF, Hernday AD. 2017. An efficient, rapid, and recyclable system for CRISPR-mediated genome editing in Candida albicans. mSphere 2 https://doi.org/10.1128/mSphereDirect.00149-17.

24. Bernardo SM, Lee SA. 2010. Candida albicans SUR7 contributes to secretion, biofilm formation, and macrophage killing. BMC Microbiol 10:133. https://doi.org/10.1186/1471-2180-10-133.

25. Rane HS, Bernardo SM, Raines SM, Binder JL, Parra KJ, Lee SA. 2013. Candida albicans VMA3 is necessary for V-ATPase assembly and function and contributes to secretion and filamentation. Eukaryot Cell 12:1369–1382. https://doi.org/10.1128/EC.00118-13.

26. Crandall M, Edwards JE. 1987. Segregation of proteinase-negative mutants from heterozygous Candida albicans. J Gen Microbiol 133:2817–2824. https://doi.org/10.1099/00221287-133-10-2817.

27. Liu H, Köhler J, Fink GR. 1994. Suppression of hyphal formation in Candida albicans by mutation of a STE12 homolog. Science 266:1723–1726. https://doi.org/10.1126/science.7992058.

28. Rollenhagen C, Agyeman H, Eszterhas S., Lee SA. 2021. Candida albicans ENT2 contributes to efficient endocytosis, cell wall integrity, filamentation, and virulence. mSphere 6. https://doi.org/10.1128/mSphere.00707-21.

29. Gil-Bona A, Reales-Calderon JA, Parra-Giraldo CM, Martinez-Lopez R, Monteoliva L, Gil C. 2016. The cell wall protein Ecm33 of Candida albicans is involved in chronological life span, morphogenesis, cell wall regeneration, stress tolerance, and host-cell interaction. Front Microbiol 7:64. https://doi.org/10.3389/fmicb.2016.00064.

30. Ramage G, López-Ribot JL. 2005. Techniques for antifungal susceptibility testing of Candida albicans biofilms. Methods Mol Med 118:71–79. https://doi.org/10.1385/1-59259-943-5:071.

31. Pringle JR, Adams AE, Drubin DG, Haarer BK. 1991. Immunofluorescence methods for yeast. Methods Enzymol 194:565–602. https://doi.org/10.1016/0076-6879(91)94043-c.

32. Rollenhagen C, Wöllert T, Langford GM, Sundstrom P. 2009. Stimulation of cell motility and expression of late markers of differentiation in human oral keratinocytes by Candida albicans. Cell Microbiol 11:946–966. https://doi.org/10.1111/j.1462-5822.2009.01303.x.

33. Losberger C, Ernst JF. 1989. Sequence of the Candida albicans gene encoding actin. Nucleic Acids Res 17:9488. https://doi.org/10.1093/nar/17.22.9488.

34. Miyasaki SH, White TC, Agabian N. 1994. A fourth secreted aspartyl proteinase gene (SAP4) and a CARE2 repetitive element are located upstream of the SAP1 gene in Candida albicans. J Bacteriol 176:1702–1710. https://doi.org/10.1128/jb.176.6.1702-1710.1994.

35. Naglik JR, Newport G, White TC, Fernandes-Naglik LL, Greenspan JS, Greenspan D, Sweet SP, Challacombe SJ, Agabian N. 1999. In vivo analysis of secreted aspartyl proteinase expression in human oral candidiasis. Infect Immun 67:2482–2490. https://doi.org/10.1128/IAI.67.5.2482-2490.1999.

36. Kurien BT, Scofield RH. 2006. Western blotting. Methods 38:283–293. https://doi.org/10.1016/j.ymeth.2005.11.007.

37. Reijnst P, Jorde S, Wendland J. 2010. Candida albicans SH3-domain proteins involved in hyphal growth, cytokinesis, and vacuolar morphology. Curr Genet 56:309–319. https://doi.org/10.1007/s00294-010-0301-7.

38. Lee JA, Robbins N, Xie JL, Ketela T, Cowen LE. 2016. Functional genomic analysis of candida albicans adherence reveals a key role for the Arp2/3 complex in cell wall remodelling and biofilm formation. PLoS Genet 12:e1006452. https://doi.org/10.1371/journal.pgen.1006452.

39. Epp E, Nazarova E, Regan H, Douglas LM, Konopka JB, Vogel J, Whiteway M. 2013. Clathrin- and Arp2/3-independent endocytosis in the fungal pathogen Candida albicans. mBio 4:e00476-13–e00413. https://doi.org/10.1128/mBio.00476-13.

40. Farmakovskaya M, Khromova N, Rybko V, Dugina V, Kopnin B, Kopnin P. 2016. E-Cadherin repression increases amount of cancer stem cells in human A549 lung adenocarcinoma and stimulates tumor growth. Cell Cycle 15:1084–1092. https://doi.org/10.1080/15384101.2016.1156268.

41. Rollenhagen C, Asin SN. 2010. IL-8 decreases HIV-1 transcription in peripheral blood lymphocytes and ectocervical tissue explants. J Acquir Immune Defic Syndr 54:463–469. https://doi.org/10.1097/QAI.0b013e3181e5e12c.

42. Vida TA, Emr SD. 1995. A new vital stain for visualizing vacuolar membrane dynamics and endocytosis in yeast. J Cell Biol 128:779–792. https://doi.org/10.1083/jcb.128.5.779.

43. Lettner T, Zeidler U, Gimona M, Hauser M, Breitenbach M, Bito A. 2010. Candida albicans AGE3, the ortholog of the S. cerevisiae ARF-GAP-encoding gene GCS1, is required for hyphal growth and drug resistance. PLoS One 5:e11993. https://doi.org/10.1371/journal.pone.0011993.

44. Raths S, Rohrer J, Crausaz F, Riezman H. 1993. end3 and end4: two mutants defective in receptor-mediated and fluid-phase endocytosis in Saccharomyces cerevisiae. J Cell Biol 120:55–65. https://doi.org/10.1083/jcb.120.1.55.

45. Naglik JR, Challacombe SJ, Hube B. 2003. Candida albicans secreted aspartyl proteinases in virulence and pathogenesis. Microbiol Mol Biol Rev 67:400–428. https://doi.org/10.1128/MMBR.67.3.400-428.2003.

46. Vasioukhin V, Bauer C, Yin M, Fuchs E. 2000. Directed actin polymerization is the driving force for epithelial cell-cell adhesion. Cell 100:209–219. https://doi.org/10.1016/s0092-8674(00)81559-7.

47. Gumbiner BM. 2005. Regulation of cadherin-mediated adhesion in morphogenesis. Nat Rev Mol Cell Biol 6:622–634. https://doi.org/10.1038/nrm1699.

48. Lee SA, Jones J, Hardison S, Kot J, Khalique Z, Bernardo SM, Lazzell A, Monteagudo C, Lopez-Ribot J. 2009. Candida albicans VPS4 is required for secretion of aspartyl proteases and in vivo virulence. Mycopathologia 167:55–63. https://doi.org/10.1007/s11046-008-9155-7.

49. Lee SA, Jones J, Khalique Z, Kot J, Alba M, Bernardo S, Seghal A, Wong B. 2007. A functional analysis of the Candida albicans homolog of Saccharomyces cerevisiae VPS4. FEMS Yeast Res 7:973–985. https://doi.org/10.1111/j.1567-1364.2007.00253.x.

50. Martin R, Hellwig D, Schaub Y, Bauer J, Walther A, Wendland J. 2007. Functional analysis of Candida albicans genes whose Saccharomyces cerevisiae homologues are involved in endocytosis. Yeast 24:511–522. https://doi.org/10.1002/yea.1489.

51. Oberholzer U, Nantel A, Berman J, Whiteway M. 2006. Transcript profiles of Candida albicans cortical actin patch mutants reflect their cellular defects: contribution of the Hog1p and Mkc1p signaling pathways. Eukaryot Cell 5:1252–1265. https://doi.org/10.1128/EC.00385-05.

52. Villar CC, Kashleva H, Nobile CJ, Mitchell AP, Dongari-Bagtzoglou A. 2007. Mucosal tissue invasion by Candida albicans is associated with E-cadherin degradation, mediated by transcription factor Rim101p and protease Sap5p. Infect Immun 75:2126–2135. https://doi.org/10.1128/IAI.00054-07.